Dynamic magnetic behavior of the mixed spin (2, 5/2) Ising system with antiferromagnetic/antiferromagnetic interactions on a bilayer square lattice

Mehmet Ertaş[†] and Mustafa Keskin

Department of Physics, Erciyes University, 38039 *Kayseri, Turkey*

(Received 18 May 2013; revised manuscript received 4 July 2013)

Using the mean-field theory and Glauber-type stochastic dynamics, we study the dynamic magnetic properties of the mixed spin (2, 5/2) Ising system for the antiferromagnetic/antiferromagnetic (AFM/AFM) interactions on the bilayer square lattice under a time varying (sinusoidal) magnetic field. The time dependence of average magnetizations and the thermal variation of the dynamic magnetizations are examined to calculate the dynamic phase diagrams. The dynamic phase diagrams are presented in the reduced temperature and magnetic field amplitude plane and the effects of interlayer coupling interaction on the critical behavior of the system are investigated. We also investigate the influence of the frequency and find that the system displays richer dynamic critical behavior for higher values of frequency than that of the lower values of it. We perform a comparison with the ferromagnetic/ferromagnetic (FM/FM) and AFM/FM interactions in order to see the effects of AFM/AFM interaction and observe that the system displays richer and more interesting dynamic critical behaviors for the AFM/AFM interaction than those for the FM/FM and AFM/FM interactions.

Keywords: dynamic magnetic behavior of a bilayer Ising system, mixed spins, glauber-type stochastic dynamics, antiferromagnetic/antiferromagnetic interactions

PACS: 05.50.+q, 05.70.Fh, 64.60.Ht, 75.10.Hk **DOI:** 10.1088/1674-1056/22/12/120507

1. Introduction

The magnetic behavior of thin films has been the subject of intensive experimental and theoretical researches in recent years because of their potential for numerous technological applications. Experimentally, the structural and magnetic properties of the thin films were investigated, such as those listed below: Fe/Ni, Fe/Co, Ni/Au, Co/Cu/$Ni_{80}Fe_{20}$, $La_{2/3}Ca_{1/3}MnO_3/SrTiO_3/YBa_2Cu_3O_{7-x}$, FePt/Fe, and Fe/TbFe, etc.[1–10] On the theoretical side, the equilibrium and nonequilibrium magnetic properties of various systems for the case of interactions on different bilayer lattices have been studied in detail (see Refs. [11]–[37] and references therein). In all of these theoretical studies, the magnetic properties of the systems were investigated for ferromagnetic/ferromagnetic (FM/FM) and antiferromagnetic/ferromagnetic (AFM/FM) interactions. On the other hand, it is well known that besides FM materials, the AFM materials also play a great role in some interesting novel magnetic properties, such as surface magneto-elastic coupling, enhanced surface magnetic moment, surface magnetic anisotropy, and giant magneto resistance.[38,39] In the magnetic sensors, the antiferromagnetic substrates have an important part. It is also promising candidate for use in spintronic devices.[40] In brief, the molecular-based antiferromagnetic materials have interesting properties which need to be investgated.[41]

Although a great amount is known about the equilibrium and nonequilibrium magnetic properties of various systems for the case of FM/FM and FM/AFM interactions on different bilayer lattices, in comparison, only a few studies have been done on the equilibrium magnetic properties of various spin Ising systems for the case of AFM/AFM interactions on a bilayer Bethe lattice.[30–32] On the other hand, as far as we know, the dynamic magnetic properties of any bilayer system for the case of AFM/AFM interactions under a time varying (sinusoidal) magnetic field have not been studied.

The purpose of the present paper is twofold. The first is to study the dynamic magnetic properties of the mixed spin (2, 5/2) Ising system to obtain the AFM/AFM interactions on the bilayer square lattice under a time varying (sinusoidal) magnetic field within the mean-field approach and Glauber-type stochastic dynamics. The set of mean-field dynamic equations is obtained by employing the Glauber transition rates. We investigate the time variation of average magnetizations to find the phases in the system and the thermal behavior of dynamic magnetizations to obtain the dynamic phase transition points as well as to characterize the nature of the dynamic phase transitions. We present dynamic phase diagrams in the reduced temperature and magnetic field amplitude plane. The effect of interlayer coupling interaction, which is related to the thickness, on the critical behavior of the system is also investigated in detail. We also investigate the influence of the frequency and find that the system displays richer dynamic critical behavior for higher values of frequency than that for the lower values of it. The second is to compare the results with the results in the mixed spin (2, 5/2) Ising system on the bilayer square lattice for the FM/FM and AFM/FM interactions[34] in order to see the effects of AFM/AFM interaction.

[†]Corresponding author. E-mail: mehmetertas@erciyes.edu.tr

© 2013 Chinese Physical Society and IOP Publishing Ltd

It is worthwhile mentioning that the reasons we choose the mixed spin (2, 5/2) Ising system are as follows: (i) The system is one of the good models to study ferrimagnetic materials because in an external magnetic field, a kind of ferromagnetic behavior may be displayed in the antiferromagnetic phase, with the absolute value of one of the sublattice magnetizations differing from that of the other sublattice, resulting in a nonzero net magnetization. (ii) The system is also one of the prototypical system that has been used for investigating the magnetic properties of molecular-based magnetic materials, such as $A\mathrm{Fe^{II}Fe^{III}}(\mathrm{C_2O_4})_3$ [$A = \mathrm{N}(n-\mathrm{C}_n\mathrm{H}_{2n+1})_4$, $n = 3$–5], (see Refs. [42]–[44], and references therein). (iii) The nonequilibrium properties of mixed spin (2, 5/2) Ising ferrimagnetic systems, in the concept of the molecular-based magnetic materials, have previously been studied using Glauber-type stochastic dynamics.[45] (iv) A magnetic hysteresis of Co-based quasi-1D ferrimagnets using the model of the mixed spins (2, 5/2) Ising chain is also examined within Glauber-type stochastic dynamics.[46,47] (v) Mixed spin-2 and spin-5/2 Ising systems give richer phase diagrams and special points than those given in other mixed spin Ising systems with different spin combinations.[48] Finally, we should also mention that as far as our search is concerned we were unable to find any real experimental systems as a bilayer film where one layer is a pure spin-2 layer, whereas the other layer is a pure spin-5/2 layer, at least up to this date.

The outline of the remaining part of this paper is as follows. In Section 2, the model and the formulation are given briefly. In Section 3, the detailed numerical results and discussion are presented. A summary and conclusion is given in Section 4.

2. Model and formulations

We consider the mixed spin (2, 5/2) Ising model on the two-layer square lattice under the oscillating magnetic field. The mixed two-layer square lattice is an extension of the one-layer version; hence one considers two identical layers of square lattices G_1 (upper layer) and G_2 (lower layer) with different spins $\sigma = 2$ with values of ± 2, ± 1, 0, and $S = 5/2$ with values of $\pm 5/2$, $\pm 3/2$, $\pm 1/2$, respectively, that are placed parallel to each other forming the bilayer square lattice. The schematic representation of the system is illustrated in Fig. 1. Each layer has N sites and interacts with its nearest-neighbor (NN) and the corresponding adjacent spins in the other layer whose sites are labeled by i, j on the lower layer and i', j' on the upper layer. Therefore, each layer of the system is also a two-sublattice system with spin variables $\sigma_i = \pm 2, \pm 1, 0$, and $\sigma_{i'} = \pm 2, \pm 1, 0$ on the sites of the sublattices A and B, respectively; and $S_j = \pm 5/2, \pm 3/2, \pm 1/2$, and $S_{j'} = \pm 5/2, \pm 3/2, \pm 1/2$ on the sites of the sublattices A and B, respectively, and the system can be described with four sublattice magnetizations or simply four magnetizations. They are introduced as follows: $m_1^A \equiv \langle \sigma_i \rangle, m_1^B \equiv \langle \sigma_j \rangle, m_2^A \equiv \langle S_{i'} \rangle, m_2^B \equiv \langle S_{j'} \rangle$, where $\langle\ \rangle$ is the thermal expectation value.

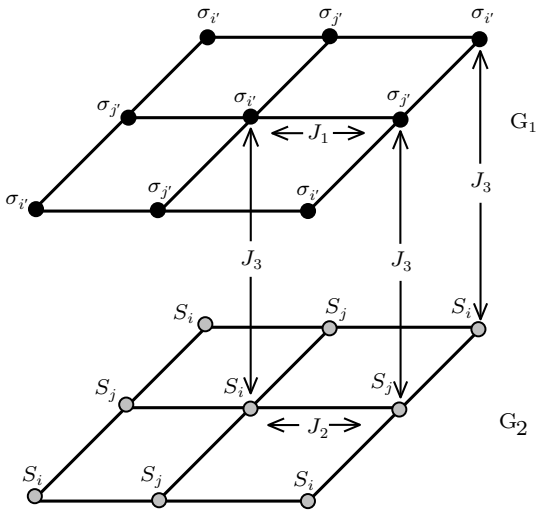


Fig. 1. Two-layer square lattice, G_1 and G_2 refer to the upper and lower layers containing the spins labeled as $\sigma_{i'}$, $\sigma_{j'}$ and S_i, S_j.

The Hamiltonian of such a mixed Ising bilayer system under a time varying (sinusoidal) magnetic field may be given as

$$\begin{aligned} H = & -J_1 \sum_{\langle i'j' \rangle} \sigma_{i'}\sigma_{j'} - J_2 \sum_{\langle ij \rangle} S_i S_j - J_3 \left(\sum_{\langle ii' \rangle} \sigma_{i'} S_i + \sum_{\langle jj' \rangle} \sigma_{j'} S_j \right) \\ & - D \left(\sum_{\langle i' \rangle} \sigma_{i'}^2 + \sum_{\langle j' \rangle} \sigma_{j'}^2 + \sum_{\langle i \rangle} S_i^2 + \sum_{\langle j \rangle} S_j^2 \right) \\ & - H(t) \left(\sum_{\langle i' \rangle} \sigma_{i'} + \sum_{\langle j' \rangle} \sigma_{j'} + \sum_{\langle i \rangle} S_i + \sum_{\langle j \rangle} S_j \right), \end{aligned} \tag{1}$$

where $\langle ij \rangle$ and $\langle i'j' \rangle$ indicate a summation over all pairs of the nearest-neighboring sites of each layer. $J_1 < 0$ and $J_2 < 0$, namely the AFM/AFM interactions, are exchange constants for the upper and lower layers, respectively, which are also called intralayer coupling constants, and J_3 is the interlayer coupling constant over all the adjacent neighboring sites of layers. D is a single-ion potential or crystal-field interaction. $H(t)$ is a time-dependent oscillating external magnetic field: $H(t) = H_0 \cos(\omega t)$, where H_0 and $\omega = 2\pi\nu$ are the amplitude and the angular frequency of the oscillating field, respectively. The system is in contact with an isothermal heat bath at absolute temperature T_{abs}.

The set of the mean-field dynamic equations of motion will be obtained by applying the Glauber-type stochastic dynamics. Since the derivations of the mean-field dynamic equations of motion of the mixed spin (2, 5/2) Ising model on the two-layer square lattice for the case of FM/FM and FM/AFM interactions within the Glauber-type stochastic dynamics were extensively described in our previous paper,[34] we have only given a brief summary here. If the spins on the sublattice B are momentarily fixed, the master equation, which describes the interaction between the spins and the heat bath, for the sublattice A can be written as

$$\begin{aligned} & \frac{\mathrm{d}}{\mathrm{d}t} P_1^A(\sigma_1^A, \sigma_2^A, \ldots, \sigma_N^A; t) \\ & = -\sum_i \left(\sum_{\sigma_i^A \neq \sigma_i^{A'}} W_i^A(\sigma_i^A \to \sigma_i^{A'}) \right) P_1^A(\sigma_1^A, \sigma_2^A, \ldots, \sigma_i^A, \ldots, \sigma_N^A; t) \end{aligned}$$

$$+\sum_i\Bigg(\sum_{\sigma_i^A\neq\sigma_i^{A'}} W_i^A(\sigma_i^{A'}\to\sigma_i^A)P_1^A(\sigma_1^A,\sigma_2^A,\ldots,\sigma_i^{A'},\ldots,\sigma_N^A;t)\Bigg), \tag{2}$$

where $W_i^A(\sigma_i^A\to\sigma_i^{A'})$ is the probability per unit time that the i-th spin changes from the values σ_i^A to $\sigma_i^{A'}$. In this sense the Glauber model is stochastic. Since the system is in contact with a heat bath at absolute temperature $T_{\rm abs}$, each spin can change from the value σ_i^A to $\sigma_i^{A'}$ with the probability per unit time by the Boltzmann factor

$$W_i^A(\sigma_i^A\to\sigma_i^{A'})=\frac{1}{\tau}\frac{\exp(-\beta\Delta E(\sigma_i^A\to\sigma_i^{A'}))}{\sum\limits_{\sigma_i^{A'}}\exp(-\beta\Delta E(\sigma_i^A\to\sigma_i^{A'}))}, \tag{3}$$

where τ is a time constant that a transition from σ_i^A to $\sigma_i^{A'}$ occurs on time scale τ, $\beta=1/k_{\rm B}T_A$, $k_{\rm B}$ being the Boltzmann factor and $\sum\limits_{\sigma_i^{A'}}$ is the sum over the five possible values of $\sigma_i^{A'}=\pm2$, ±1, 0. Moreover,

$$\begin{aligned}\Delta E_i^A(\sigma_{i'}^A\to\sigma_{i'}^{A'}) &= -(\sigma_{i'}^{A'}-\sigma_{i'}^A)\Big(J_1\sum_{j'}\sigma_{j'}^B+J_3\sum_i S_i^A+H\Big)\\ &\quad-\big((\sigma_{i'}^{A'})^2-(\sigma_{i'}^A)^2\big)D,\end{aligned} \tag{4}$$

gives the change in the energy of the system when the σ_i-spin changes. The probabilities satisfy the detailed balance condition. Using Eqs. (2), (3), and (4) with the mean-field approach, we obtain the average mean-field dynamic equations for the sublattice A on the upper layer G_1

$$\Omega\frac{\mathrm{d}}{\mathrm{d}\xi}m_1^A=-m_1^A+\frac{2\exp\Big(\frac{4d}{T}\Big)\sinh\Big[\frac{2}{T}\Big(zm_1^B+\frac{J_3}{J_1}m_2^A+h\cos\xi\Big)\Big]+\exp\Big(\frac{d}{T}\Big)\sinh\Big[\frac{1}{T}\Big(zm_1^B+\frac{J_3}{J_1}m_2^A+h\cos\xi\Big)\Big]}{\exp\Big(\frac{4d}{T}\Big)\cosh\Big[\frac{2}{T}\Big(zm_1^B+\frac{J_3}{J_1}m_2^A+h\cos\xi\Big)\Big]+\exp\Big(\frac{d}{T}\Big)\sinh\Big[\frac{1}{T}\Big(zm_1^B+\frac{J_3}{J_1}m_2^A+h\cos\xi\Big)\Big]+1/2}, \tag{5}$$

where $m_1^A\equiv\langle\sigma_{i'}^A\rangle$, $m_1^B\equiv\langle\sigma_{j'}^B\rangle$, $m_2^A\equiv\langle S_i^A\rangle$, $m_2^B\equiv\langle S_j^B\rangle$, $\xi=wt$, $T=(\beta J_1)^{-1}$, $h=H_0/J_1$, $d=D/J_1$, and $\Omega=\tau w$. We fixed $\tau=1$, $z=4$, and $w=2\pi\nu$.

Now, assuming that the spins on the sublattice A remain momentarily fixed and that the spins on the sublattice B change, we obtain the average mean-field dynamic equations for the sublattice B on the upper layer G_1 as

$$\Omega\frac{\mathrm{d}}{\mathrm{d}\xi}m_1^B=-m_1^B+\frac{2\exp\Big(\frac{4d}{T}\Big)\sinh\Big[\frac{2}{T}\Big(zm_1^A+\frac{J_3}{J_1}m_2^B+h\cos\xi\Big)\Big]+\exp\Big(\frac{d}{T}\Big)\sinh\Big[\frac{1}{T}\Big(zm_1^A+\frac{J_3}{J_1}m_2^B+h\cos\xi\Big)\Big]}{\exp\Big(\frac{4d}{T}\Big)\cosh\Big[\frac{2}{T}\Big(zm_1^A+\frac{J_3}{J_1}m_2^B+h\cos\xi\Big)\Big]+\exp\Big(\frac{d}{T}\Big)\sinh\Big[\frac{1}{T}\Big(zm_1^A+\frac{J_3}{J_1}m_2^B+h\cos\xi\Big)\Big]+1/2}. \tag{6}$$

The other mean-field dynamic equations for m_2^A and m_2^B on the lower layer G_2 can be similarly calculated as

$$\begin{aligned}\Omega\frac{\mathrm{d}}{\mathrm{d}\xi}m_2^A &= -m_2^A+\Big\{5\sinh\Big[\frac{5}{2T}\Big(\frac{J_2}{J_1}zm_2^B+\frac{J_3}{J_1}m_1^A+h\cos\xi\Big)\Big]+3\exp\Big(-\frac{4d}{T}\Big)\sinh\Big[\frac{3}{2T}\Big(\frac{J_2}{J_1}zm_2^B+\frac{J_3}{J_1}m_1^A+h\cos\xi\Big)\Big]\\ &\quad+\exp\Big(-\frac{6d}{T}\Big)\sinh\Big[\frac{1}{2T}\Big(\frac{J_2}{J_1}zm_2^B+\frac{J_3}{J_1}m_1^A+h\cos\xi\Big)\Big]\Big\}\times\Big\{2\cosh\Big[\frac{5}{2T}\Big(\frac{J_2}{J_1}zm_2^B+\frac{J_3}{J_1}m_1^A+h\cos\xi\Big)\Big]\\ &\quad+2\exp\Big(-\frac{4d}{T}\Big)\cosh\Big[\frac{3}{2T}\Big(\frac{J_2}{J_1}zm_2^B+\frac{J_3}{J_1}m_1^A+h\cos\xi\Big)\Big]+\exp\Big(-\frac{6d}{T}\Big)\cosh\Big[\frac{1}{2T}\Big(\frac{J_2}{J_1}zm_2^B+\frac{J_3}{J_1}m_1^A+h\cos\xi\Big)\Big]\Big\}^{-1},\end{aligned} \tag{7}$$

$$\begin{aligned}\Omega\frac{\mathrm{d}}{\mathrm{d}\xi}m_2^B &= -m_2^B+\Big\{5\sinh\Big[\frac{5}{2T}\Big(\frac{J_2}{J_1}zm_2^A+\frac{J_3}{J_1}m_1^B+h\cos\xi\Big)\Big]+3\exp\Big(-\frac{4d}{T}\Big)\sinh\Big[\frac{3}{2T}\Big(\frac{J_2}{J_1}zm_2^A+\frac{J_3}{J_1}m_1^B+h\cos\xi\Big)\Big]\\ &\quad+\exp\Big(-\frac{6d}{T}\Big)\sinh\Big[\frac{1}{2T}\Big(\frac{J_2}{J_1}zm_2^A+\frac{J_3}{J_1}m_1^B+h\cos\xi\Big)\Big]\Big\}\times\Big\{2\cosh\Big[\frac{5}{2T}\Big(\frac{J_2}{J_1}zm_2^A+\frac{J_3}{J_1}m_1^B+h\cos\xi\Big)\Big]\\ &\quad+2\exp\Big(-\frac{4d}{T}\Big)\cosh\Big[\frac{3}{2T}\Big(\frac{J_2}{J_1}zm_2^A+\frac{J_3}{J_1}m_1^B+h\cos\xi\Big)\Big]+\exp\Big(-\frac{6d}{T}\Big)\cosh\Big[\frac{1}{2T}\Big(\frac{J_2}{J_1}zm_2^A+\frac{J_3}{J_1}m_1^B+h\cos\xi\Big)\Big]\Big\}^{-1}.\end{aligned} \tag{8}$$

Thus, we obtained a set of coupled mean-field dynamic equations, and the numerical solutions and discussion of these equations are given in Section 3.

3. Numerical results and discussion

3.1. Time variations of average magnetizations

In order to find the phases in the system, we have to study the stationary solutions of the set of coupled mean-field dynamic equations for magnetizations, namely given in Eqs. (5)–(8), when the parameters T, J_1, J_2, J_3, d, and h are varied. J_1 and J_2 are always taken as $J_1<0$ and $J_2<0$, i.e. the AFM/AFM interaction. The stationary solutions of Eqs. (5)–(8) will be periodic functions of ξ with period 2π, that is, $m^{A,B}(\xi+2\pi)=m^{A,B}(\xi)$. Moreover, they can be one of three types according to whether they have or do not have the properties

$$m_1^A(\xi+\pi)=-m_1^A(\xi)\quad\text{and}\quad m_1^B(\xi+\pi)=-m_1^B(\xi), \tag{9a}$$

and

$$m_2^A(\xi+\pi)=-m_2^A(\xi)\quad\text{and}\quad m_2^B(\xi+\pi)=-m_2^B(\xi). \tag{9b}$$

The stationary solutions of Eqs. (5)–(8) gave the paramagnetic (p) that is a dynamically disordered phase as well as the ferromagnetic (f), antiferromagnetic phase (af), mixed

(m), and non-magnetic (nm) which are dynamically ordered phases. In addition to these fundamental phases, we have also found the f + p, af + m, m + p, f + nm, nm + p, f + m + p, and af + m + nm dynamically coexistence phase regions. Since the obtaining of these phases for the FM/FM and FM/AFM interactions has been given in detail,[34] we will not discuss the solutions or present any figures here. We only summarize or illustrate these phases in Table 1.

Table 1. Characteristics of time variations of magnetizations $m_1^A(\xi)$, $m_1^B(\xi)$, $m_2^A(\xi)$, $m_2^B(\xi)$.

			Oscillation of sublattice magnetizations
Fundamental phases or solutions	p		$m_1^A = m_1^B = m_2^A = m_2^B = 0$
	f		$m_1^A = m_1^B \neq 0$ and with positive spin values $m_2^A = m_2^B \neq 0$ and with positive spin values
	m		$m_1^A = -m_1^B,\ m_2^A = -m_2^B$
	af		$m_1^A = -m_1^B,\ -m_2^A = m_2^B$
	nm		$m_1^A = m_1^B = 0,\ m_2^A = m_2^B \neq 0$ or $m_1^A = m_1^B \neq 0,\ m_2^A = m_2^B = 0$
Coexistence phases or solutions	f+p	f	$m_1^A = m_1^B \neq 0$ and with positive spin values $m_2^A = m_2^B \neq 0$ and with positive spin values
		p	$m_1^A = m_1^B = m_2^A = m_2^B = 0$
	f+m	f	$m_1^A = m_1^B \neq 0$ and with positive spin values $m_2^A = m_2^B \neq 0$ and with positive spin values
		m	$m_1^A = -m_1^B,\ m_2^A = -m_2^B$
	af+m	af	$m_1^A = -m_1^B,\ -m_2^A = m_2^B$
		m	$m_1^A = -m_1^B,\ m_2^A = -m_2^B$
	m+p	m	$m_1^A = -m_1^B,\ m_2^A = -m_2^B$
		p	$m_1^A = m_1^B = m_2^A = m_2^B = 0$
	nm+p	nm	$m_1^A = m_1^B = 0,\ m_2^A = m_2^B \neq 0$ or $m_1^A = m_1^B \neq 0,\ m_2^A = m_2^B = 0$
		p	$m_1^A = m_1^B = m_2^A = m_2^B = 0$
	f+m+p	f	$m_1^A = m_1^B \neq 0$ and with positive spin values $m_2^A = m_2^B \neq 0$ and with positive spin values
		m	$m_1^A = -m_1^B,\ m_2^A = -m_2^B$
		p	$m_1^A = m_1^B = m_2^A = m_2^B = 0$
	af+m+nm	af	$m_1^A = -m_1^B,\ -m_2^A = m_2^B$
		m	$m_1^A = -m_1^B,\ m_2^A = -m_2^B$
		nm	$m_1^A = m_1^B = 0,\ m_2^A = m_2^B \neq 0$ or $m_1^A = m_1^B \neq 0,\ m_2^A = m_2^B = 0$

3.2. Thermal behavior of dynamic magnetizations

In this subsection, we investigate the behavior of the average magnetizations in a period or the dynamic magnetizations as a function of reduced temperature. This investigation leads us to obtain the dynamic phase transition (DPT) points as well as to characterize the nature (continuous or discontinuous) of the dynamic phase transitions. The dynamic magnetizations, $M_1^{A,B}$ and $M_2^{A,B}$, are defined as

$$M_1^A = \frac{1}{2\pi}\int_0^{2\pi} m_1^A(\xi)\mathrm{d}\xi, \quad M_1^B = \frac{1}{2\pi}\int_0^{2\pi} m_1^B(\xi)\mathrm{d}\xi, \tag{10}$$

and

$$M_2^A = \frac{1}{2\pi}\int_0^{2\pi} m_2^A(\xi)\mathrm{d}\xi, \quad M_2^B = \frac{1}{2\pi}\int_0^{2\pi} m_2^B(\xi)\mathrm{d}\xi. \tag{11}$$

To obtain the DPT points as well as to characterize the nature of the dynamic boundaries, the thermal behaviors of $M_1^{A,B}$ and $M_2^{A,B}$ for several values of the interaction parameters are obtained by solving Eqs. (10) and (11). We solve these equations by combining the numerical methods of the Adams–Moulton predictor corrector with Romberg integration. We fixed J_1, J_2, d, h and changed J_3 in order to see the effect of interlayer coupling interaction on the critical behavior of the system. We should also point out that J_3 is related to the thickness. If J_3 is small that means the thickness is small, otherwise it is big. A few explanatory and interesting examples are plotted in Figs. 2(a)–2(c) in order to illustrate the calculation of the DPT points and the dynamic phase boundaries among the phases. In these figures, T_C and T_t are the critical or the second-order phase transition and the first-order phase transition temperatures, respectively. Figure 2(a) shows the behaviors of dynamic magnetizations, $M_1^{A,B}$ and $M_2^{A,B}$, as functions of the reduced temperature for $J_1 = -0.2$, $J_2 = -0.1$, $d = 0.1$, $h = 0.1$, and $J_3 = 0.1$. In the figure, $M_1^A = 2.0$, $M_2^B = 5/2$, and $M_1^A = -2.0$, $M_2^B = 5/2$ at zero absolute temperature, and M_1^A, M_2^A decrease and M_1^B, M_2^B increase to zero discontinuously as the reduced temperature increases; hence a first-order phase transition occurs at $T_t = 1.790$. The phase transition is from the m to the p phases that is clearly observed in Fig. 3(c) for $h = 0.1$. In this case, the solution does not depend on the initial values of $M_1^{A,B}$ and $M_2^{A,B}$. Figure 2(b) illustrates the thermal variations $M_1^{A,B}$ and $M_2^{A,B}$ for $J_1 = -0.2$, $J_2 = -0.1$, $d = 0.1$, $h = 0.3$, and $J_3 = 0.75$ for two different initial values; i.e., $M_1^A = M_1^B = 2$ for the dashed lines and $M_2^A = M_2^B = 5/2$ for the solid lines. From this figure, one can see that below T_{t1} the f + m phase, between T_{t1} and T_{t2} the m + p phase, and above T_{t2} the p phase exists. Therefore, the system undergoes two successive first-order phase transitions, the first one is from the f + m phase to the m + p phase at $T_{t1} = 0.501$, and the second

one is from the m + p to the p phase at $T_{t2} = 3.360$. This fact is also seen clearly in Fig. 3(e) for $h = 0.3$. Figure 2(c) displays the temperature dependence of $M_1^{A,B}$ and $M_2^{A,B}$ for $J_1 = -0.2$, $J_2 = -0.1$, $d = 0.1$, $h = 0.15$, and $J_3 = 5.0$ for two different initial values; i.e., $M_1^A = M_1^B = 2$ for the dashed lines and $M_2^A = M_2^B = 5/2$ for the solid lines. This case is exactly similar to the previous case, i.e., the case for Fig. 2(b), except the system undergoes two successive second-order phase transitions at $T_{C1} = 3.700$ and $T_{C2} = 6.450$ in which the first one is from the f + m phase to m + p phase at $T_{C1} = 3.700$ and the second one is from the m + p to the p phase at and $T_{C2} = 6.450$. This fact is also seen clearly in Fig. 3(g) for $h = 0.15$. In the last two cases, the solutions depend on the initial values of $M_1^{A,B}$ and $M_2^{A,B}$. From these investigations we concluded that if J_3 is small, the system generally undergoes a first-order phase transition, otherwise a second-order one.

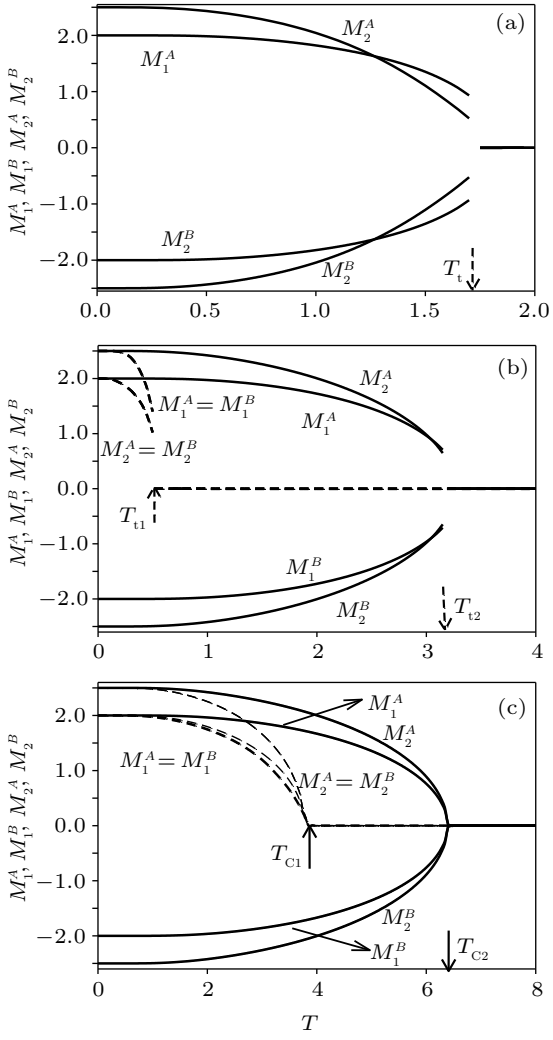


Fig. 2. Reduced temperature dependences of dynamic magnetizations M_1^A, M_1^B and M_2^A, M_2^B. T_C and T_t are the critical or the second-order phase transition and the first-order phase transition temperatures, respectively. (a) Exhibiting first-order phase transition from the m phase to the p phase for $J_1 = -0.2$, $J_2 = -0.1$, $d = 0.1$, $h = 0.1$, and $J_3 = 0.1$. T_t is found at 1.790. (b) Exhibiting two successive first-order phase transitions, the first one is from the f + m phase to the m + p phase at $T_{t1} = 0.501$, and the second one is from the m + p to the p phase at $T_{t2} = 3.360$ for $J_1 = -0.2$, $J_2 = -0.1$, $d = 0.1$, $h = 0.3$, and $J_3 = 0.75$ for two different initial values; i.e., $M_1^A = M_1^B = 2$ for the dashed lines and $M_2^A = M_2^B = 5/2$ for the solid lines. (c) Exhibiting two successive second-order phase transitions, the first one is from the f + m phase to the m + p phase at $T_{C1} = 3.700$, and the second one is from the m + p to the p phase at $T_{C2} = 6.450$ for $J_1 = -0.2$, $J_2 = -0.1$, $d = 0.1$, $h = 0.3$, and $J_3 = 0.75$ for two different initial values; i.e., $M_1^A = M_1^B = 2$ for the dashed lines and $M_2^A = M_2^B = 5/2$ for the solid lines.

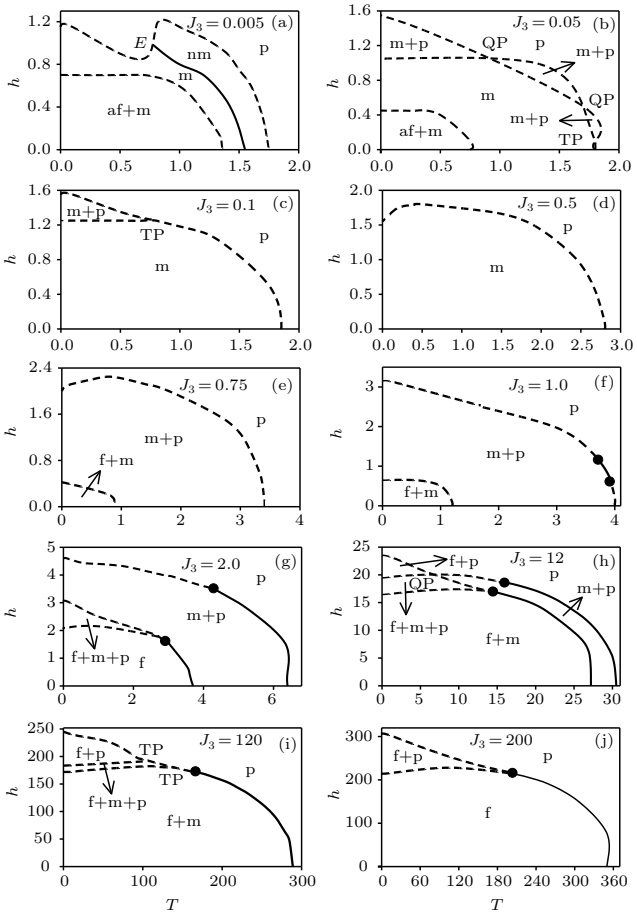


Fig. 3. Phase diagrams of mixed spin (2, 5/2) Ising system on two-layer square lattice in (T, h) plane for antiferromagnetic/antiferromagnetic (AFM/AFM) interactions ($J_1 < 0$ and $J_2 < 0$), $J_1 = -0.2$, $J_2 = -0.1$, $d = 0.1$, and $h = 0.1$. The solid and dashed lines represent the second- and first-order phase transition lines, respectively, and the dynamic tricritical point is denoted by a filled circle. E, TP, and QP represent the dynamic critical end point, triple point, and quadruple point, respectively. (a) $J_3 = 0.005$; (b) $J_3 = 0.05$; (c) $J_3 = 0.1$; (d) $J_3 = 0.5$; (e) $J_3 = 0.75$; (f) $J_3 = 1.0$; (g) $J_3 = 2.0$; (h) $J_3 = 12.0$; (i) $J_3 = 120.0$; (j) $J_3 = 200.0$.

3.3. Dynamic phase diagrams

Since we have obtained the DPT points, in Subsection 3.2, we can now present the dynamic phase diagrams of the system. The calculated phase diagrams in the (T, h) planes are presented in Figs.3–5, for various values of the interaction parameters. In these phase diagrams, the solid and dashed lines represent the second- and first-order phase transition lines, respectively, and the dynamic tricritical point is denoted by a filled circle. E, TP, and QP represent the dynamic critical end point, triple point, and quadruple point, respectively. The system displays the p dynamically disordered phase, the f, af, m, and nm dynamically disordered phases

and seven different dynamically coexistence phases which are composed of a binary and ternary combination of dynamically disordered and ordered phases, strongly depending on the interaction parameters, in particular on J_3.

The dynamic phase diagram of the mixed Ising model for the case of AFM/AFM interactions on the bilayer square lattice for $J_1 = -0.2$, $J_2 = -0.1$, $d = 0.1$, $h = 0.1$, and various values of J_3 are shown in Fig. 3 and ten main different topological types of dynamic phase diagrams are found. In Fig. 3, the following six interesting phenomena are seen. (i) For $0.045 > J_3 \geq 0.0$, the dynamic phase boundaries among the phases are first-order phase lines, but the boundary between the m and nm phases is a second-order and the system also exhibits the dynamic critical end point (E). (ii) For $0.084 > J_3 \geq 0.915$, the system always undergoes a first-order phase transition; hence all dynamic phase boundaries among the phases are first-order lines. (iii) For $1.850 > J_3 \geq 0.915$, the phase diagrams exhibit two dynamic tricritical points and for a small T and large h the system undergoes a first-order phase transition, otherwise either a first- or second-order depending on T and h values. (iv) For $48.20 > J_3 \geq 1.850$, the system also displays two dynamic tricritical points and for small T and large h values the system undergoes a first-order phase transition, otherwise always a second-order phase transition. (v) For $J_3 \geq 48.20$, the phase diagram is similar to the previous case, except the dynamic phase boundary between the m + p and p phases disappeared; hence the system exhibits only one dynamic tricritical point. (vi) In Figs. 3(a), 3(d), and 3(e), the system exhibits re-entrant behavior, i.e., as the temperature is increased, the system passes from the dynamically disordered paramagnetic (p) phase to the dynamically ordered m phase as shown in Fig. 3(d) and the p phase passes to the m + p phase as shown in Fig. 3(e) and back to the p phase again for high values of h. In spin systems, re-entrant behavior can be perceived as follows. At high temperatures, entropy is the most important factor and uncorrelated fluctuations determine the thermodynamics. The system is then in the disordered phase bias due to the applied field. As the temperature is lowered, the energy and entropy are both important and the correlated fluctuations affect the dominance of either phase significantly; hence the system enters the ordered phase. At low temperatures, the energy is important, not the entropy, and the system re-enters the disordered phase again.[49,50]

Figure 4 illustrates the dynamic phase diagrams in the (T,h) plane for $J_1 = -0.2$, $J_2 = -0.1$, $d = -0.5$, $h = 0.1$, and various values of J_3; six main types of phase diagrams are observed. From these phase diagrams, which have negative values of crystal field interaction, the following five interesting phenomena were found. i) For $0.1 > J_3 \geq 0.0$, the system exhibits one dynamic tricritical point and for small T and large h values the system undergoes a first-order phase transition, otherwise either a first- or second-order depending on T and h values, as seen in Fig. 4(a). ii) For $0.5 > J_3 \geq 0.1$, the phase diagram also displays one dynamic tricritical point and for small T and large h values the system undergoes a first-order phase transition, otherwise always a second-order phase transition, as illustrated in Fig. 4(b). iii) For $J_3 \geq 0.5$, the system illustrates two dynamic tricritical points and for small T and large h values, the system undergoes a first-order phase transition, otherwise always a second-order phase transition, as seen in Figs. 4(c)–4(f). iv) In Figs. 4(c) and 4(d) the system exhibits re-entrant behavior or that is the same as in Fig. 3(e). v) For large values of J_3, the system exhibits richer phase diagrams.

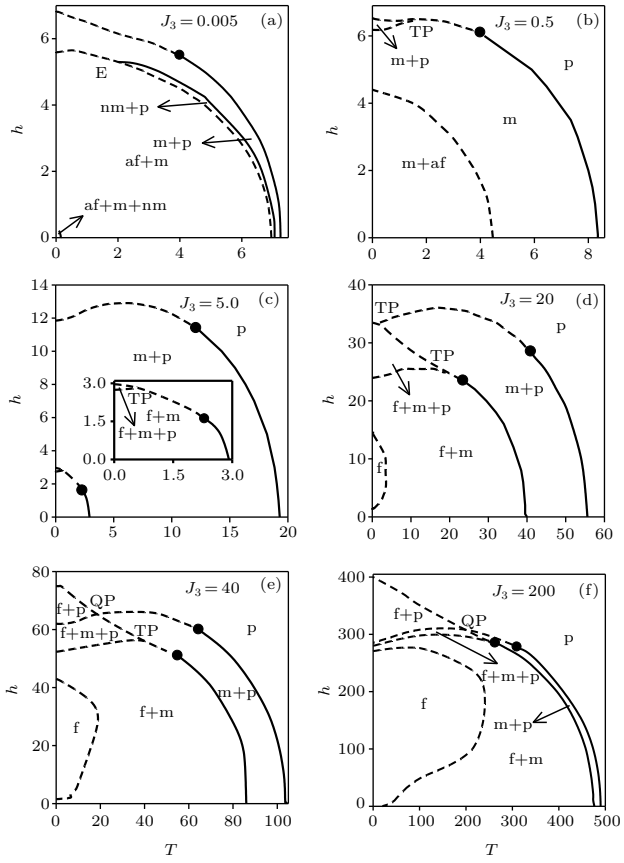


Fig. 4. Same as Fig. 3, but for $J_1 = -0.2$, $J_2 = -0.1$, $d = -0.5$, $h = 0.1$. (a) $J_3 = 0.005$; (b) $J_3 = 0.05$; (c) $J_3 = 5.0$; (d) $J_3 = 20.0$; (e) $J_3 = 40.0$; (f) $J_3 = 200.0$.

Since the case of AFM/FM with $J_1 > 0$ and $J_2 < 0$ is not examined in Ref. [34], we study the case of AFM/FM for $J_1 > 0$ and $J_2 < 0$; nine main types of phase diagrams are observed and presented in Fig. 5. The following features can be singled out in Fig. 5. a) The dynamic phase boundary is always first-order lines; hence the system does not exhibit dynamic tricritical behavior as seen in Fig. 5(a). b) The system includes one dynamic, two, and three dynamic tricritical points, as seen in Figs. 5(c)–5(f); 5(g); 5(h), 5(i), respectively. c) The system displays one TP dynamic special point, as seen in Figs. 5(b), 5(c), 5(e), 5(i). Moreover one Z dynamic zero-temperature critical point appears in Fig. 5(d). d) The dynamic phase diagrams contain f, c, nm, sf, and p fundamental phases and the f + p, f + nm, c + p, sf + c, sf + nm, and f + nm + p mixed phases. e) The dynamic phase boundaries among the phases are mostly first-order phase lines except the dynamic phase boundary among the fundamental phases.

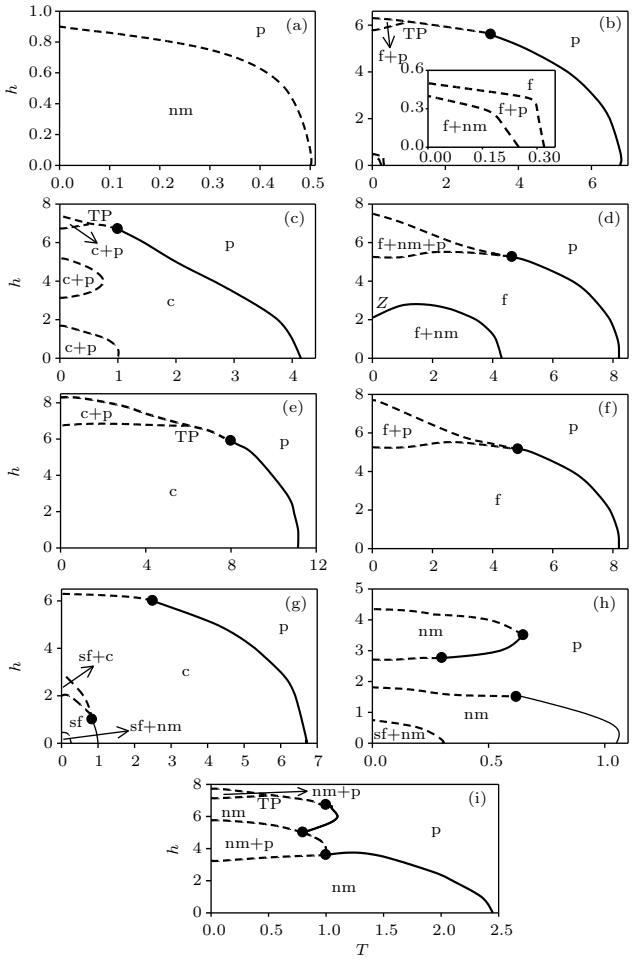


Fig. 5. Same as Fig. 3, but for antiferromagnetic/ferromagnetic (AFM/FM) interactions ($J_1 > 0$ and $J_2 < 0$), $J_1 = 1$ and (a) $J_2 = -0.5$, $J_3 = 0.1$, $d = -4$; (b) $J_2 = -0.2$, $J_3 = 1$, $d = -1$; (c) $J_2 = -0.1$, $J_3 = -0.1$, $d = -1.8$; (d) $J_2 = -0.1$, $J_3 = 0.1$, $d = 0.1$; (e) $J_2 = -0.2$, $J_3 = -2$, $d = 1$; (f) $J_2 = -0.5$, $J_3 = 0.1$, $d = 0.1$; (g) $J_2 = -0.5$, $J_3 = -1$, $d = -1$; (h) $J_2 = -1$, $J_3 = 0.7$, $d = -3$; (i) $J_2 = -0.5$, $J_3 = 0.1$, $d = -2$.

We also investigate the influence of the frequency and present two dynamic phase diagrams for two different values of ω, namely $\omega = 0.1\pi$ and $\omega = 10\pi$, as seen in Figs. 6(a) and 6(b). We find that the system displays richer dynamic critical behavior for higher values of frequency than that for the lower values of it. These figures correspond to Fig. 3(h) calculated for $J_1 = -0.2$, $J_2 = -0.1$, $J_3 = 12$, $d = 0.1$, $h = 0.1$, and $\omega = 2\pi$. If one compares Fig. 6(a) with Fig. 3(b), one can see that the system exhibits only the m + p mixed phase besides the f and p fundamental phases, two dynamic tricritical points and one triple point, as seen in Fig. 6(a); hence the system gives a simple dynamic critical behavior. On the other hand, for large values of ω, the system exhibits richer and interesting dynamic critical behaviors, such as three dynamic tricritical points, the QP special point, and two f fundamental phases that appear for low values of T and h, by comparing Fig. 3(h) with Fig. 6(b).

Finally, in order to see the effects of AFM/AFM interaction we should compare these dynamic phase diagrams with the dynamic phase diagrams, namely Figs. 4–7, in Ref. [34] in which both the FM/FM and AFM/FM interactions were considered. By comparisons, the following interesting differences have been observed: (I) The system with the AFM/AFM interaction exhibits richer and interesting dynamic phase diagrams than the system with both the FM/FM and AFM/FM interactions. (II) The system with AFM/AFM interaction displays the dynamic re-entrant behavior for both positive and negative values of the single-ion potential, but the system with the FM/FM and AFM/FM interactions illustrates only negative values of the single-ion potential. (III) The dynamic phase transition points and dynamic special points as well as dynamic tricritical points occur at higher temperatures for the AFM/AFM interaction than the FM/FM and AFM/FM interactions. (IV) The compensated (c) and the surface (sf) fundamental phases do not exist for the AFM/AFM interaction, but it occurs for the FM/FM and AFM/FM interactions. (V) The system does not display the Z dynamic zero-temperature critical point for the AFM/AFM interaction, but it exists for the AFM/FM interactions.

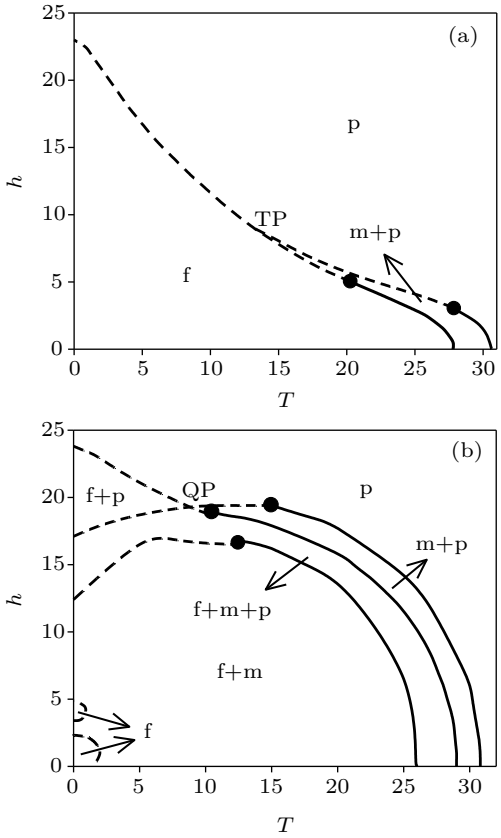


Fig. 6. Same as Fig. 3, but for $J_1 = -0.2$, $J_2 = -0.1$, $d = 0.1$, $h = 0.1$, and (a) $\omega = 0.1\pi$, (b) $\omega = 10\pi$.

4. Summary and conclusion

In a summary, we analyzed within a mean-field approach, the dynamic magnetic properties of the mixed spin (2, 5/2) Ising system with antiferromagnetic/antiferromagnetic (AFM/AFM) and AFM/FM with $J_1 > 0$, $J_2 < 0$ interactions on the bilayer square lattice under the presence of a time varying (sinusoidal) magnetic field ($H = H_0 \cos(\omega t)$) by using Glauber-type stochastic dynamics. The dynamic phase diagrams are presented in the reduced temperature and magnetic field amplitude plane and the effects of interlayer cou-

pling interaction on the critical behavior of the system are investigated. We also investigate the influence of the frequency and find that the system displays richer dynamic critical behavior for higher values of frequency than that for the lower values of it. Finally, we perform a comparison with the same system for the FM/FM and AFM/FM with $J_1 < 0$ and $J_2 > 0$ interactions[34] and AFM/FM with $J_1 > 0$ and $J_2 < 0$ interactions. We find that the system with the AFM/AFM interaction exhibits richer and more interesting dynamic critical behaviors than the system with the FM/FM and AFM/FM interactions. Moreover, the dynamic phase transition points and dynamic special points exist at higher temperatures with the AFM/AFM interaction than those with the FM/FM and AFM/FM interactions. Finally, we hope that our detailed theoretical investigation may stimulate further works to study the dynamic magnetic properties of more complicated bilayer systems with AFM/AFM interactions on molecular-based magnetic materials and may shed some light on future experimental researches.

References

[1] Dawber M, Rabe K M and Scott J F 2005 *Rev. Mod. Phys.* **77** 1083
[2] Edelstein A D, Kim C, Quadri S B, Kim K H, Browning V, Yu H Y, Murayama B and Everett K 1990 *Solid State Commun.* **76** 1379
[3] Jennet N M and Dingley D J 1991 *J. Magn. Magn. Mater.* **93** 472
[4] Colombo E, Donzelli O, Fraatucello G B and Ronconi F 1992 *J. Magn. Magn. Mater.* **107** 1857
[5] Krishnan R, Gupta H O, Lassri H, Sella C and Kaaboutchi J 1991 *J. Appl. Phys.* **70** 6421
[6] Bayreuther G, Bensch F and Kottler V 1996 *J. Appl. Phys.* **79** 4509
[7] Chou K W, Puzic A, Stoll H, Schütz G, Waeyenberge B V, Tyliszczak T, Rott K, Reiss G, Brückl H, Neudecker I, Weiss D and Back C H 2006 *J. Appl. Phys.* **99** 08F305
[8] Yashwant G, Prajapat C L, Ravikumar G, Soltan S, Christiani G and Habermeier H U 2012 *J. Magn. Magn. Mater.* **324** 1406
[9] Huang L S, Hu J F and Chen J S 2012 *J. Magn. Magn. Mater.* **324** 1242
[10] Li J 2012 *J. Magn. Magn. Mater.* **324** 1512
[11] Kaneyoshi T 1989 *Phys. Rev. B* **40** 2529
[12] Jiang Q and Li Z Y 1989 *J. Magn. Magn. Mater.* **80** 178
[13] Landau D P and Binder K 1990 *Phys. Rev. B* **41** 4786
[14] Krishnan R, Gupta H O, Lassri H, Sella C and Kaaboutchi J 1991 *J. Appl. Phys.* **70** 6421
[15] Jaščur M and Bobák A 1992 *Phys. Rev. B* **45** 9722
[16] Bayreuther G, Bensch F and Kottler V 1996 *J. Appl. Phys.* **79** 4509
[17] Jang H and Grimson M J 2001 *Phys. Rev. E* **63** 066119
[18] Jang H, Grimson M and Hall C K 2003 *Phys. Rev. B* **67** 094411
[19] Jang H, Grimson M and Woolf T B 2004 *Phys. Rev. E* **70** 047101
[20] ChouK W, Puzic A, Stoll H, Schütz G, Waeyenberge B V, Tyliszczak T, Rott K, Reiss G, Brückl H, Neudecker I, Weiss D and Back C H 2006 *J. Appl. Phys.* **99** 08F305
[21] Canko O and Albayrak E 2007 *Phys. Rev. E* **75** 011116
[22] Canko O, Kantar E and Keskin M 2009 *Physica A* **388** 28
[23] Balcerzak T and Łuźniak I 2009 *Physica A* **388** 357
[24] Ekiz C 2008 *Physica A* **387** 1185
[25] Yashwant G, Prajapat C L, Ravikumar G, Soltan S, Christiani G and Habermeier H U 2012 *J. Magn. Magn. Mater.* **324** 1406
[26] Pan L, Li H J, WenY W, TanX J, Lü H Y, Shi J and Tang X F 2011 *Phys. Lett. A* **375** 614
[27] AkıncıÜ 2013 *J. Magn. Magn. Mater.* **329** 178
[28] Li J 2012 *J. Magn. Magn. Mater.* **324** 1512
[29] Oitmaa J R R and Singh P 2012 *Phys. Rev. B* **85** 014428
[30] Albayrak E and Akkaya S 2009 *Phys. Scr.* **79** 065005
[31] Albayrak E, Akkaya S and Cengiz T 2009 *J. Magn. Magn. Mater.* **321** 3726
[32] Albayrak E and Yigit A 2009 *Chin. Phys. B* **18** 1674
[33] Gomonay H V, Kunitsyn R V and Loktev V M 2012 *Phys. Rev. B* **85** 134446
[34] Ertaş M and Keskin M 2012 *Phys. Lett. A* **376** 2455
[35] Essaoudi I, Bärner K, Ainane A and Saber M 2007 *Physica A* **385** 208
[36] Wei G, Zhang Q, Xin Z and Liang Y 2004 *J. Magn. Magn. Mater.* **277** 1
[37] Zhang Q, Wei G, Xin Z and Liang Y 2004 *J. Magn. Magn. Mater.* **280** 14
[38] Baibich M N, Broto J M, Fert A, Nguyen Van Dau F, Petroff F, Etienne P, Creuzet G, Friederich A and Chazelas J 1988 *Phys. Rev. Lett.* **61** 2472
[39] Camley R E and Barna J 1989 *Phys. Rev. Lett.* **63** 664
[40] Gomonay H V, Kunitsyn R V and Loktev V M 2012 *Phys. Rev. B* **85** 134446
[41] Bhattacharjee B, Miyazaki Y and Sorai M 2004 *J. Magn. Magn. Mater.* **280** 1
[42] Kaneyoshi T, Nakamura Y and Shin S 1999 *J. Phys.: Condens. Matter* **10** 7025
[43] Nakamura Y 2000 *Phys. Rev. B* **62** 11742
[44] Li J, Du A and Wei G 2004 *Physica B* **348** 79
[45] Bukharov A A, Ovchinnikov A S, Baranov N V and Inoune K 2009 *Eur. Phys. J. B* **70** 369
[46] Ertaş M, Keskin M and Deviren B 2012 *J. Stat. Phys.* **146** 1244
[47] Ertaş M, Keskin M and Deviren B 2012 *Physica A* **391** 1038
[48] Ertaş M and Keskin M 2009 *Phys. Rev. E* **80** 061140
[49] Keskin M, Pınar M A, Erdinç A and Canko O 2006 *Physica A* **364** 263
[50] Hui K 1988 *Phys. Rev. B* **38** 802